The Meteoritical Society

Meteoritics & Planetary Science 45, Nr 12, 1889–1905 (2011)
doi: 10.1111/j.1945-5100.2010.01126.x

A NanoSIMS and Auger Nanoprobe investigation of an isotopically primitive interplanetary dust particle from the 55P/Tempel-Tuttle targeted stratospheric dust collector

Christine FLOSS[1*], Frank J. STADERMANN[1], Aaron F. MERTZ[1,2], and Thomas J. BERNATOWICZ[1]

[1]Laboratory for Space Sciences and Physics Department, Washington University, One Brookings Drive, St. Louis, Missouri 63130, USA
[2]Department of Physics, Yale University, P.O. box 208120, New Haven, Connecticut 06520, USA
[*]Corresponding author. E-mail: floss@wustl.edu

(Received 18 December 2009; revision accepted 17 September 2010)

Abstract–An IDP nicknamed Andric, from a stratospheric dust collector targeted to collect dust from comet 55P/Tempel-Tuttle, contains five distinct presolar silicate and/or oxide grains in 14 ultramicrotome slices analyzed, for an estimated abundance of approximately 700 ppm in this IDP. Three of the grains are ^{17}O-enriched and probably formed in low-mass red giant or asymptotic giant branch (AGB) stars; the other two grains exhibit ^{18}O enrichments and may have a supernova origin. Carbon and N isotopic analyses show that Andric also exhibits significant variations in its N isotopic composition, with numerous discrete ^{15}N-rich hotspots and more diffuse regions that are also isotopically anomalous. Three ^{15}N-rich hotspots also have statistically significant ^{13}C enrichments. Auger elemental analysis shows that these isotopically anomalous areas consist largely of carbonaceous matter and that the anomalies may be hosted by a variety of components. In addition, there is evidence for dilution of the isotopically heavy components with an isotopically normal endmember; this may have occurred either as a result of extraterrestrial alteration or during atmospheric entry. Isotopically primitive IDPs such as Andric share many characteristics with primitive meteorites such as the CR chondrites, which also contain isotopically anomalous carbonaceous matter and abundant presolar silicate and oxide grains. Although comets are one likely source for the origin of primitive IDPs, the presence of similar characteristics in meteorites thought to come from the asteroid belt suggests that other origins are also possible. Indeed the distinction between cometary and asteroidal sources is somewhat blurred by recent observations of icy comet-like planetesimals in the outer asteroid belt.

INTRODUCTION

Interplanetary dust particles (IDPs) are complex assemblages of primitive solar system materials. In past work (Floss et al. 2006; Stadermann et al. 2006), we have shown that circumstellar and interstellar phases are concentrated in a subgroup of isotopically primitive IDPs. These particles, which are characterized by anomalous bulk N isotopic compositions, typically contain abundant ^{15}N-rich hotspots and occasional C isotopic anomalies (Floss et al. 2004, 2006). It has been suggested that these types of anomalies may have originated through ion-molecule reactions in cold molecular clouds (e.g., Messenger et al. 2003a). Isotopically primitive IDPs also have high abundances of presolar silicate grains (approximately 375 ppm; Floss et al. 2006), and the first presolar aluminum oxide and silicon carbide grains found in IDPs were identified from an isotopically primitive IDP (Stadermann et al. 2006). The particles from these studies included both individual IDPs and fragments from so-called "cluster" IDPs (e.g., Messenger 2000)

Table 1. Interplanetary dust particles measured in this study.

Nickname	Collector	Particle	Collection[a]	Slices[b]	Size (μm^2)[c]
Andric	U2108	B2	T-T	14	4×8
Perse	U2121	Cluster 2 B2	G-S	15	7×10
Quasimodo	L2055	Cluster 5 B3	G-S	1	5×9

[a]T-T = Tempel-Tuttle; G-S = Grigg-Skjellerup.
[b]Number of slices obtained from the IDP.
[c]Maximum dimensions of the slices.

and were randomly selected from several different stratospheric collectors.

Recently there has been a focus on targeted collections, stratospheric dust collectors flown at specific times designed to coincide with the passage of the Earth through the dust trails of specific comets, in the hopes of collecting enhanced quantities of cometary dust over background extraterrestrial materials. Particles from the stratospheric dust collectors L2054, L2055, U2120, and U2121, which were flown in April 2003 as part of a targeted collection designed to coincide with the passage of the Earth through the dust trail of comet 26P/Grigg-Skjellerup (Messenger 2002), have been of particular interest. Although these collectors will have sampled IDPs from many sources in addition to the targeted comet, and it is still uncertain exactly how to identify the Grigg-Skjellerup particles (solar flare tracks and noble gas measurements are two possibilities), a significant fraction of IDPs from these collectors are isotopically primitive, with large D and ^{15}N enrichments and high abundances of presolar grains (Busemann et al. 2009). In addition, there is evidence for unusual noble gas signatures in some particles (Palma et al. 2005).

Statistical comparisons of IDPs from targeted collections with those from nontargeted collectors provide the opportunity to assess whether there are significant differences between populations and can provide constraints on genetic relationships among different types of extraterrestrial particles. Here we report on three IDPs selected from targeted collections. Two of the particles come from collectors which targeted the comet 26P/Grigg-Skjellerup dust trail in April 2003 while the other is a particle from a collector flown in November 2002 in an attempt to collect Leonid storm debris from comet 55P/Tempel-Tuttle (Rietmeijer et al. 2003). Preliminary data were reported by Floss et al. (2007, 2010).

EXPERIMENTAL

We selected three IDPs for a detailed NanoSIMS and Auger spectroscopy study (Table 1). In order to maximize the surface area available for analysis, we prepared multiple sliced sections of these IDPs. The particles were mounted in resin and sliced with a diamond ultramicrotome, following procedures established for preparing presolar graphite grains for transmission electron microscopy (TEM) analysis (Croat et al. 2003). However, the slices were thicker than conventional TEM sections (nominally approximately 200 nm) in order to provide sufficient material for multiple, sequential isotopic measurements, and were deposited on high purity Si wafers which provided a stable substrate for the lengthy NanoSIMS analyses. The samples were coated with a thin (approximately 20 Å) layer of Au to prevent charging. Multiple slices were produced for two of the three IDPs; only a single slice was produced from the third IDP, due to a malfunction of the ultramicrotome (Table 1).

Isotopic measurements were made with the Washington University NanoSIMS in multicollection raster ion imaging mode (e.g., Floss et al. 2006) with an approximately 1 pA Cs^+ primary ion beam (approximately 100 nm diameter), and consisted of two series of measurements, one for O ($^{16}O^-$, $^{17}O^-$, $^{18}O^-$, $^{28}Si^-$, $^{24}Mg^{16}O^-$ or $^{27}Al^{16}O^-$) and one for C and N ($^{12}C^-$, $^{13}C^-$, $^{12}C^{14}N^-$, $^{12}C^{15}N^-$, $^{28}Si^-$). The raster areas ranged in size from 5×5 to 11×11 μm^2, depending on the size of the IDP slice being analyzed, and acquisition rates ranged between 3 and 5 ms per pixel. Each imaging measurement consisted of between 20 and 40 scans that were subsequently added together to constitute a single image measurement of 256^2 pixels. Synthetic SiC ($^{12}C/^{13}C = 92.1$) and Si_3N_4 ($^{14}N/^{15}N = 272$) were used as standards for the C and N isotopic measurements, while O isotopic compositions were normalized internally assuming standard solar oxygen ratios ($^{16}O/^{17}O = 2625$; $^{16}O/^{18}O = 499$) for bulk IDP compositions (Floss et al. 2006).

The IDP slices and various components therein were further characterized for their elemental makeup with the Washington University PHI 700 Auger Nanoprobe. Details of the procedures are described by Floss and Stadermann (2009a, 2009b). Auger electron energy spectra were obtained with a 10 kV 0.25 nA primary electron beam, which was rastered over grains of interest; sizes of the rastered areas were typically

between 100 and 300 nm. Multiple spectral scans of a given grain are added together to obtain a single Auger spectrum, which is differentiated using a 7-point Savitsky-Golay smoothing and differentiation routine prior to peak identification and quantification. These analysis protocols (low beam current, beam rastering, and repeated spectra acquisition) were established to reduce the possibility of electron beam damage on fragile presolar silicate grains, which can occasionally produce artifacts (e.g., compositional changes) in the Auger spectra (Stadermann et al. 2009), and have been adopted as our standard operating procedures. Sensitivity factors for O, Si, Fe, Mg, Ca, and Al were obtained from olivine and pyroxene standards of various compositions (Stadermann et al. 2009). Carbon and N sensitivity factors were obtained by least-squares fitting of the Auger intensities to the C abundances and N/C ratios of a set of terrestrial kerogen standards (Hayes et al. 1983). The C concentrations of the kerogens range from 64 to 77 wt%, and have nominal N/C ratios that span an order of magnitude (0.002–0.021). Estimated 1σ uncertainties are based on these standards and are: O: 3.6%; Si: 11.0%; Fe: 11.2%; Mg: 9.4%; Ca: 10.8%; Al: 24.9%; C: 11.0%; and N: 11.0%. These errors are lower limits and do not take into account other factors that can affect the quality of the data, such as sample charging, contributions from background noise and extrapolation of sensitivity factors to compositions significantly different from those of the standards. The Auger Nanoprobe was only installed in our laboratory after completion of the NanoSIMS work on these IDPs and the two presolar grains characterized by Auger spectroscopy in this study were measured before our standard protocol was implemented. Because we cannot be sure that the higher beam currents (10 nA) used to measure these grains did not damage them, we do not provide quantitative data for these grains. High-resolution (10–20 nm) Auger elemental distribution maps of selected elements (C, N, O, S, Mg, Fe, and Si) were obtained for selected slices and regions after acquisition of the Auger spectra. Mapping was carried out at 10 kV with a 5 nA primary beam and consisted of 5–20 scans over the area of interest for most elements, but up to 70 scans for N, due to the low signal of this element.

RESULTS

Presolar Silicate/Oxide Grains

Oxygen isotopes were measured in 13 slices of Perse, 14 slices of Andric, and the single slice of Quasimodo; two slices of Perse could not be measured because of ion optical effects due to their proximity to the edge of the Si wafer. No presolar grains were found in the slice of Quasimodo, nor in any of the slices of Perse, comprising a total area of 330 μm^2. However, in Andric, where we measured a total area of 165 μm^2, we found five distinct O-anomalous presolar grains in four different slices (Fig. 1). Three of the grains have ^{17}O-rich compositions consistent with an O isotope "group 1" classification, and likely formed in the outflows of low-mass red giant or asymptotic giant branch (AGB) stars (Nittler et al. 1997). The other two grains are ^{18}O-rich and belong to "group 4" (Nittler et al. 1997); these grains may have supernova origins, as recently suggested by Nittler et al. (2008). Although the three group 1 grains have virtually identical O isotopic compositions (Table 2, Fig. 1), based on their locations in the slices, they all appear to be distinct grains, rather than slices of the same grain. Two of them occur in different parts of the same slice, and the position of the third in its slice does not align with either of the other two. NanoSIMS secondary electron (SE) images also show that all three presolar grains are embedded in the surrounding IDP matrix, indicating that their original positions have not been altered by the slicing process.

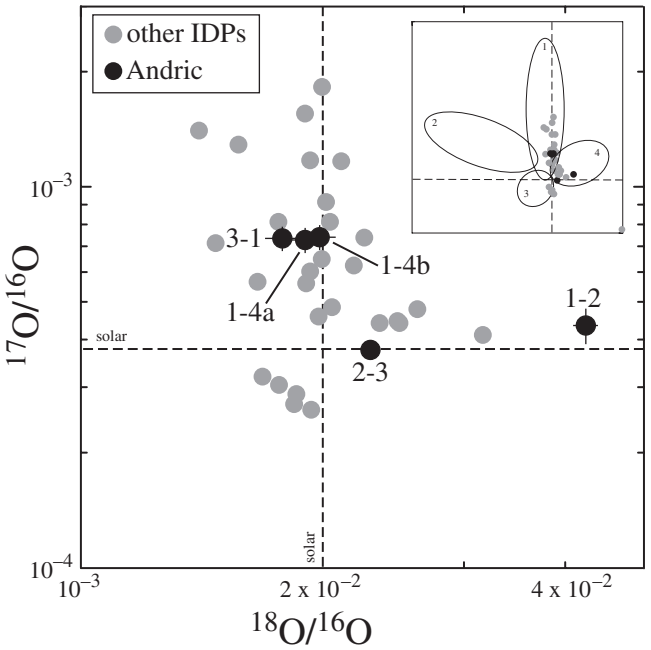

Fig. 1. Oxygen three isotope plot showing O-anomalous grains from Andric (black circles) and other IDPs (gray dots). IDP data are from Messenger et al. (2003b, 2005), Floss et al. (2006), Stadermann et al. (2006), and Busemann et al. (2009). The inset shows the data on a wider scale in relation to O isotope group designations established by Nittler et al. (1997) for presolar oxide grains. Analytical 1σ uncertainties, shown only for the Andric data, are in some cases smaller than the symbols. Dashed lines indicate normal (solar) O isotopic ratios.

Table 2. Oxygen isotopic compositions of presolar grains from the IDP Andric.

Grain[a]	Group	Size (nm)[b]	$^{17}O/^{16}O$ ($\times10^{-4}$)[c]	$^{18}O/^{16}O$ ($\times10^{-3}$)[c]
1–2	4	190 × 220	4.36 ± 0.47	4.24 ± 0.15
1–4a	1	160 × 200	7.31 ± 0.56	1.90 ± 0.09
1–4b	1	125	7.44 ± 0.56	1.98 ± 0.09
2–3	4	125 × 250	3.76 ± 0.19	2.29 ± 0.05
3–1	1	125 × 150	7.38 ± 0.54	1.78 ± 0.09

[a]Designation refers to the wafer and specific slice in which the presolar grain is found (note that the numbering does not imply adjacent slices); two grains were found in slice 1–4.
[b]Estimated from NanoSIMS ion images except for 1–4a and 2–3.
[c]Errors are 1σ.

Based on the total area analyzed in the 14 slices (as determined from the NanoSIMS ion images), the calculated abundance of presolar grains in Andric is 700 ± 300 ppm. The upper limit on the abundance of presolar grains in Perse is 30 ppm.

Portions of only two of the presolar grains, 1–4a and 2–3, were still present after the NanoSIMS analyses for characterization with the Auger Nanoprobe. Figure 2 shows SE images and elemental distribution maps for both grains. Grain 1–4a is about 160 × 200 nm in size and has a smooth platy appearance. The elemental maps, as well as a spot analysis, indicate that it is a ferromagnesian silicate that contains subequal amounts of Mg and Fe in addition to Si and O. Grain 2–3 is an elongate grain 125 × 250 nm in dimension. The spot analysis confirms that it is also a silicate, but compositionally it is more Fe-rich with only a minor contribution from Mg; it also contains S (Fig. 2). The presence of Fe associated with S could indicate a GEMS (glass with embedded metal and sulfides; Bradley 1994) particle; however, the grain does not appear to have the aggregate texture often associated with GEMS (cf. Fig. 12 of Floss et al. 2006).

Carbon and Nitrogen Compositions and Distributions

Carbon and nitrogen isotopes were measured in the single slice of Quasimodo and in 11 slices each of Perse and Andric; they were not measured in the two slices that contained remaining portions of the O-rich presolar grains found in Andric, nor in several slices that did not contain sufficient remaining material after the O imaging measurements. All slices of Perse and the single slice of Quasimodo have normal bulk compositions for both C and N; in addition, no C-anomalous or N-anomalous hotspots were observed in these IDPs. In contrast, anomalous isotopic compositions in both C and N are seen in Andric (Table 3; Figs. 3 and 4).

Individual slices of Andric have normal C isotopic compositions (Table 3), but exhibit significant variations in their N isotopic compositions (Fig. 3). The slices contain both discrete ^{15}N-rich hotspots and larger, more diffuse regions that are also isotopically anomalous, but with lower maximum ^{15}N enrichments. The average N isotopic compositions of individual slices range from essentially normal up to $\delta^{15}N = +400‰$ (Table 3; Fig. 4). Although the distinction between ^{15}N-enriched diffuse regions and ^{15}N-rich hotspots is somewhat arbitrary, the latter are typically more localized and are characterized by higher ^{15}N enrichments ($\delta^{15}N = +525$ to $+945‰$). Three of the ^{15}N-rich hotspots (2–6 hs1, 3–2 hs2 and 3–3 hs1) are accompanied by statistically significant C isotopic anomalies (Table 3; Fig. 4). One of these (3–3 hs1) is among the most ^{15}N-rich of the hotspots observed in Andric, with a $\delta^{15}N$ of $+940‰$. Auger data on two of these grains (2–6 hs1 and 3–3 hs1; see below) suggest that SiC is not the carrier of the C isotopic anomalies. Figure 4 also shows that C and N isotopes appear to be correlated in Andric: although most samples have normal C isotopic compositions within the errors, there is a trend toward increasingly heavy C as ^{15}N enrichments increase. The possible significance of this trend is discussed below.

We obtained Auger elemental spectra from four hotspots (1–6 hs1, 1–6 hs2, 2–6 hs1, 3–3 hs1), which did not sputter away during the NanoSIMS measurements; the compositions of these four hotspots are shown in Table 4 and Fig. 5. We also analyzed a number of other isotopically anomalous regions in eight of the Andric slices with Auger spectroscopy; like the hotspots, these areas are ^{15}N-rich, but are more diffuse than areas defined as hotspots and they generally have lower $\delta^{15}N$ values (e.g., Fig. 3). The ranges in elemental compositions are summarized in Table 4 and are shown graphically in Fig. 5, together with the compositions of the hotspots. Both the hotspots and the diffuse areas in Andric are dominated by O, Si, and C, but lesser amounts of Mg, Fe, S, and N are also present in most regions. Abundances vary significantly, with factor of five variations in the major elements. The compositions of the four ^{15}N-rich hotspots fall within the ranges observed for other isotopically anomalous regions of Andric, and contain between 25 and 40 atom% C, with variable N abundances (2–9 atom%). Low Si abundances and the presence of Mg, Fe, and S, in addition to C, in 2–6 hs1 and 3–3 hs1 (Table 4) suggest that these C- and N-anomalous hotspots are not SiC, but rather consist of carbonaceous matter intimately associated with silicates and sulfides.

The presence of Si, Mg, Fe, and S in the hotspots and other isotopically anomalous areas indicates that

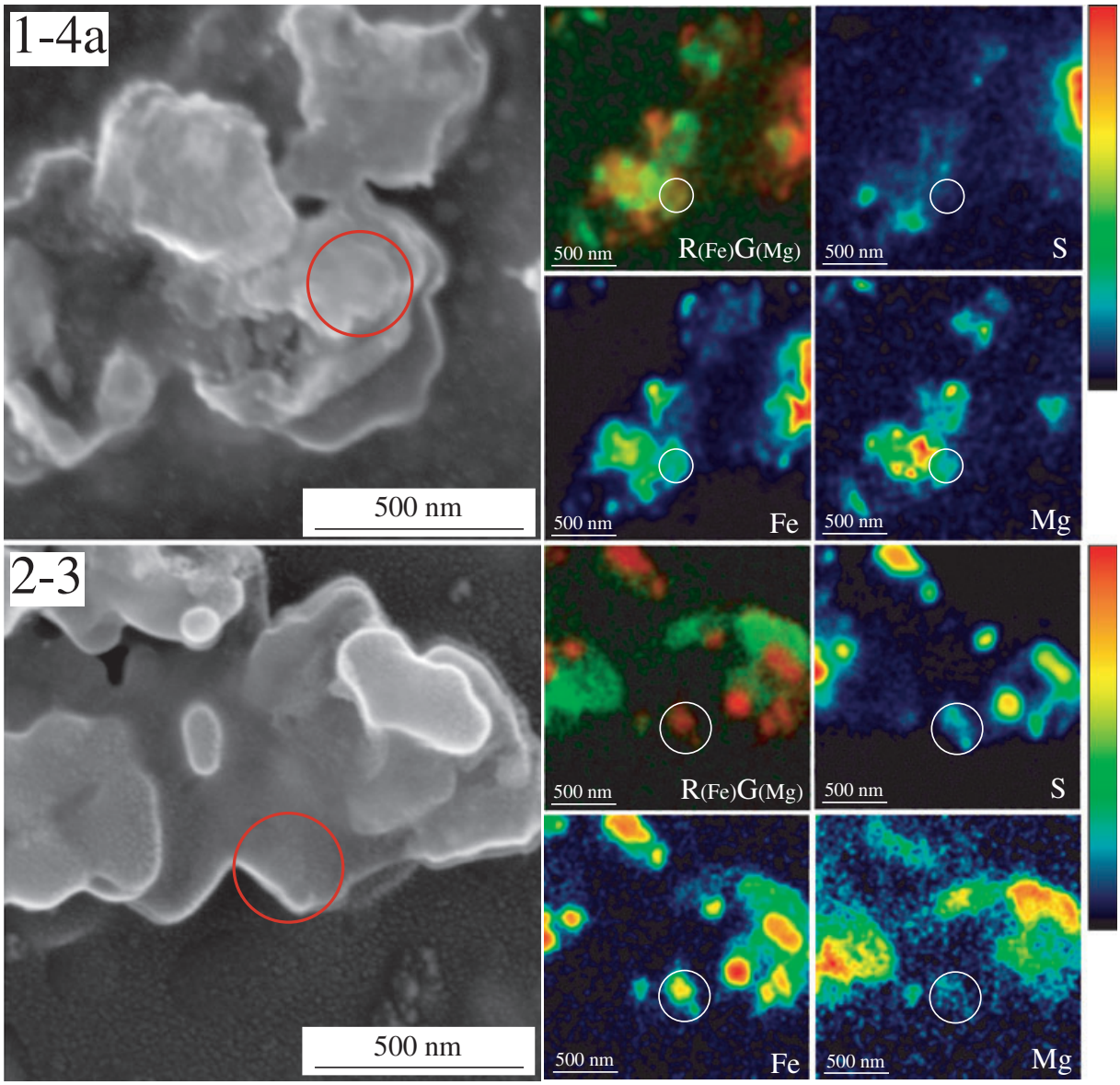

Fig. 2. Secondary electron images and Auger elemental distribution maps of presolar grains from IDP Andric. Top: grain 1–4a; bottom: grain 2–3. Note that the scales of the elemental maps are somewhat different from the SE images. The RG images show the abundances of Fe and Mg in red and green, respectively.

these analyses generally represent mixtures of the silicate material, sulfides and carbonaceous matter typically found in IDPs. In addition, there may be some contribution from the Si wafer substrate on which the IDP slices are mounted, as these samples have been extensively sputtered in the NanoSIMS and in many cases little material appears to be left. Because of this possible contribution from the Si wafer, and because we are primarily interested in characterizing the carbonaceous components that are the likely hosts of the N and C isotopic anomalies, we also show in Table 4 renormalized elemental compositions representing the carbonaceous material present in each of the areas analyzed. These compositions were calculated from the bulk compositions assuming that only C, N, and O are present in the carbonaceous material. This assumption is not strictly correct, as some of the O measured is undoubtedly associated with the silicate material present in these areas. However, a deconvolution of the O abundances into silicate and carbonaceous components has not been attempted due to the difficulties associated with accurately determining and assigning values to the separate components. Thus, the renormalized O concentrations shown in Table 4 should be considered upper

Table 3. Carbon and nitrogen isotopic compositions in the IDP Andric.

Sample[a]	$^{12}C/^{13}C$[b]	$\delta^{13}C$ (‰)[b,c]	$^{14}N/^{15}N$[b]	$\delta^{15}N$ (‰)[b,c]	CN^-/C^-	Size (nm)[d]
Bulk 1–1	88.8 ± 3.0	2 ± 34	221 ± 11	228 ± 62	0.77	
Bulk 1–2	88.8 ± 3.0	2 ± 34	234 ± 12	163 ± 58	0.75	
Bulk 1–3	91.8 ± 3.1	−30 ± 33	230 ± 12	184 ± 59	0.64	
Bulk 1–5	89.3 ± 3.0	−3 ± 34	214 ± 11	273 ± 63	0.83	
Bulk 1–6	95.4 ± 3.3	−67 ± 32	246 ± 12	107 ± 55	1.41	
Bulk 2–1	89.5 ± 0.8	−5 ± 9	274 ± 14	−9 ± 49	0.40	
Bulk 2–4	90.8 ± 1.0	−20 ± 11	268 ± 14	15 ± 52	1.16	
Bulk 2–5	90.7 ± 0.9	−19 ± 10	271 ± 14	5 ± 51	0.94	
Bulk 2–6	87.8 ± 0.8	14 ± 9	196 ± 10	391 ± 69	1.30	
Bulk 3–2	87.4 ± 0.6	19 ± 7	207 ± 6	316 ± 39	0.79	
Bulk 3–3	88.1 ± 0.6	10 ± 7	203 ± 6	340 ± 40	0.81	
1–5 hs1	87.7 ± 3.3	15 ± 38	156 ± 8	742 ± 93	1.12	375 × 400
1–5 hs2	85.7 ± 3.1	39 ± 38	150 ± 8	817 ± 96	0.84	250 × 400
1–6 hs1	91.6 ± 3.9	−28 ± 41	169 ± 9	607 ± 90	1.50	250 × 340
1–6 hs2	87.6 ± 4.5	16 ± 53	166 ± 11	638 ± 113	1.19	190 × 190
2–1 hs1	88.9 ± 2.1	1 ± 23	179 ± 11	524 ± 90	0.53	190 × 220
2–1 hs2	86.8 ± 1.7	25 ± 20	178 ± 10	525 ± 84	0.73	275 × 380
2–6 hs1	84.7 ± 1.3	50 ± 16	157 ± 8	733 ± 88	1.99	330 × 375
3–2 hs1	86.4 ± 1.5	30 ± 17	152 ± 5	786 ± 63	1.04	310 × 400
3–2 hs2	84.6 ± 0.8	52 ± 10	160 ± 5	704 ± 53	0.83	650 × 720
3–3 hs1	79.1 ± 1.4	125 ± 20	140 ± 5	939 ± 68	1.34	220 × 310
3–3 hs2	85.0 ± 1.4	47 ± 17	140 ± 6	944 ± 88	0.28	150 × 150

[a]Designation refers to the wafer and specific slice measured (note that the numbering does not imply adjacent slices); "hs" refers to hotspots in a given slice; "bulk" indicates the entire slice.
[b]Errors are 1σ.
[c]Deviation from normal ($^{12}C/^{13}C$ = 89; $^{14}N/^{15}N$ = 272) in parts per thousand.
[d]Estimated from NanoSIMS ion images.

limits to the true O abundances in the carbonaceous material. Some S could also be present in the carbonaceous matter, but the amount is likely to be small and, thus, its exclusion does not have a significant effect on the calculations. The recalculated compositions suggest a wide range of C concentrations, from 25 to 85 atom%, and N abundances from 2 to 19 atom%. Carbon concentrations for the hotspots fall in the middle of this range; two of the hotspots have distinctly high N concentrations (approximately 16 atom%), while the other two have lower N abundances of 3–5 atom% (Table 4).

In addition to obtaining elemental spectra, we acquired C and N Auger elemental maps of slice 3–3 of Andric, the section with the most anomalous ^{15}N-rich hotspots. Figure 6 shows the N isotopic composition of this slice, along with the C and N elemental distributions. Although hotspot 2 was sputtered away prior to the Auger measurements, the elemental maps show that material from hotspot 1, which is anomalous in both N and C (Table 3), contains both C and N. The elemental maps show that although C and N are both present in most areas of the slice, there are some exceptions, such as the region indicated by the arrow in Fig. 6, which contains some N, but little to no C.

DISCUSSION

Presolar Grains in IDPs

Andric contains 700 ± 300 ppm of O-anomalous presolar grains, nominally a factor of two more than the approximately 375 ppm abundance of such grains in the subgroup of isotopically primitive IDPs (Floss et al. 2006), although within errors the abundances are not different. Quoted abundances in IDPs exhibit a wide range, from 120 ppm for the suite of 25 IDPs studied by Floss et al. (2006) to as high as 15,000 ppm for the single IDP L2054 G4 (Busemann et al. 2009). As discussed in more detail below, IDPs probably originate from a variety of sources and, therefore, a range of presolar grain abundances is not unexpected, given that the degree to which pristine early nebular material is preserved is likely to be variable as well. In addition, however, the calculated abundances are also dependent on the selection criteria used to include or exclude various samples. For example, Floss et al. (2006) noted that the abundance of O-anomalous presolar grains in the subgroup of isotopically primitive IDPs is 375 ppm, although the abundance of all IDPs they analyzed is only 120 ppm. Similarly, Busemann et al. (2009) find

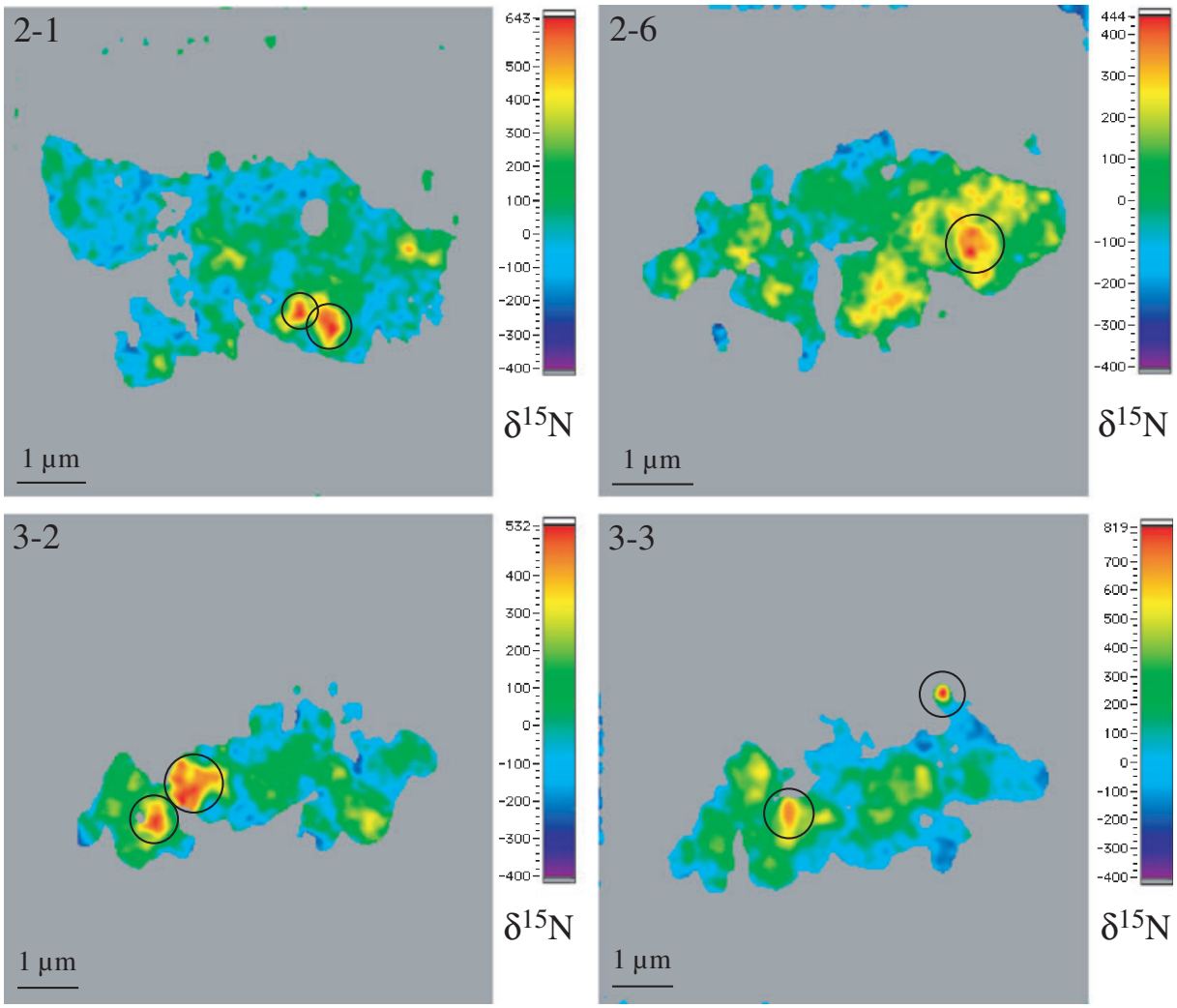

Fig. 3. False-color images of the N isotopic compositions (expressed in permil deviations from normal) in different slices of the IDP Andric. The slices contain both discrete ^{15}N-rich hotspots (red areas; circled) and larger, more diffuse ^{15}N-rich regions (green to yellow areas). Note that the scale is different for each slice.

abundances of 15,000 ppm and 3,500 ppm in two different IDPs from collector L2054, but an abundance of only 500 ppm in all the IDPs they analyzed from this collector. Yada et al. (2008) also found an order of magnitude difference in the abundances calculated for Antarctic micrometeorites (AMMs), depending on whether all or only some AMMs were considered.

Calculated abundances of O-anomalous grains in the most extensively studied primitive meteorites [Acfer 094, Allan Hills [ALH] 77307, Queen Alexandra Range (QUE) 99177, and Meteorite Hills (MET) 00426] are generally on the order of 150–200 ppm (Nguyen et al. 2007; Floss and Stadermann 2009a; Vollmer et al. 2009), less than most estimates for IDPs. These averages are obtained from statistically significant sampling of large areas of matrix material, which generally vastly exceeds the available surface area of any given IDP or groups of several IDPs, even if ultramicrotome slices are analyzed. However, heterogeneities in the abundances also exist in different portions of some primitive meteorites. Floss and Stadermann (2009a) found that different matrix areas in the QUE 99177 CR3 chondrite have different abundances of O-anomalous grains, ranging from 90 to 335 ppm. Floss and Stadermann (2009c) observed similar variations in the ungrouped carbonaceous chondrite Adelaide. It is not yet clear whether these differences arise from heterogeneities in the reservoirs from which these meteorites accreted or whether they are the result of variable secondary processing in the meteorites themselves. However, the presence of such variability in samples known to come from a single parent body emphasizes the need for

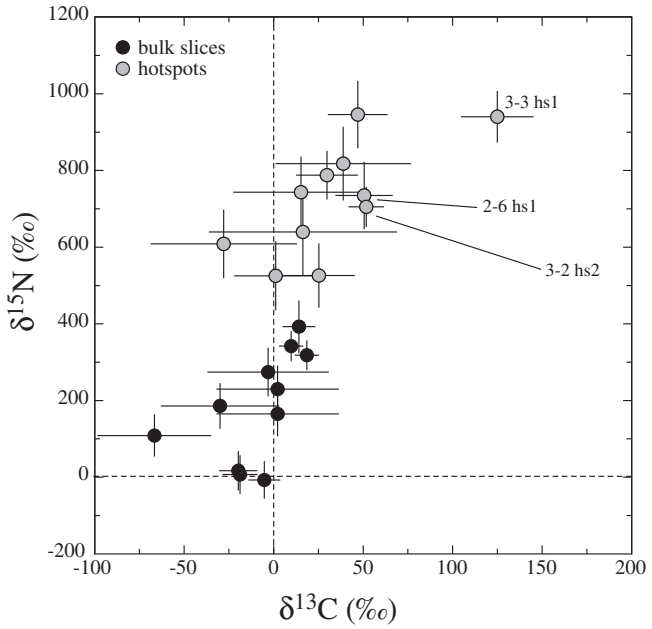

Fig. 4. Carbon and N isotopic compositions (expressed as permil deviations from normal) in bulk slices of Andric (black circles) and discrete ^{15}N-rich hotspots within individual slices (gray circles). Three hotspots with anomalous C isotopic compositions are labeled. Errors are 1σ.

caution when evaluating the accuracy of abundance estimates obtained from small samples such as IDPs or micrometeorites.

The presence of multiple presolar grains in IDP Andric appears to be a common feature of primitive IDPs. In our earlier work we also found several IDPs with multiple O-anomalous presolar grains (Floss et al. 2006); the number of such particles was likely a lower limit, as these IDPs were pressed as single particles into Au foil and significant amounts of material typically remained after the NanoSIMS O isotopic measurements, which could have hosted additional, undetected presolar grains. A similar observation was made by Busemann et al. (2009), who found four and seven O-anomalous grains, respectively, in two primitive IDPs. Clustering of presolar grains has also been observed in AMMs (Yada et al. 2008) and in primitive carbonaceous chondrites (Floss and Stadermann 2009a; Vollmer et al. 2009). In some cases the grains that are clustered together have similar isotopic compositions, such as the three group 1 grains of Andric or the presence of four rare group 3 grains in one IDP, as observed by Busemann et al. (2009). In other cases, however, multiple grains with notably different isotopic compositions, requiring distinct stellar sources, have been found in close proximity (e.g., Floss and Stadermann 2009a). The extraterrestrial samples in which these grains are found often also contain carbonaceous matter with C and/or N isotopic anomalies (e.g., Floss et al. 2004, 2006, 2009; Floss and Stadermann 2009a, 2009b, 2009d; Busemann et al. 2009) that likely represents material formed by low-temperature chemical reactions in cold molecular clouds (see below). The preservation of this material in samples from parent bodies that are traditionally thought to have formed in distinct regions of the solar nebula suggests incomplete homogenization of the molecular cloud material from which the solar system formed and large-scale transport of matter within the solar system (e.g., Ciesla 2009), as has also been suggested to explain the presence of high temperature phases in the material returned by the Stardust mission from comet 81P/Wild 2 (Brownlee et al. 2006; McKeegan et al. 2006; Zolensky et al. 2006).

Finally, Yada et al. (2008) noted that the proportion of ^{18}O-enriched group 4 silicate and oxide grains in AMMs and IDPs is significantly greater than that in primitive meteorites (33–37% versus approximately 11%). In this study two of the five presolar grains found belong to group 4; although the numbers are small, this distribution is consistent with these earlier observations. Group 4 grains are thought to originate from one or more supernovae (Nittler 2007; Nittler et al. 2008), and it has been suggested that the overabundance of these grains in IDPs and AMMs, compared to primitive meteorites, could reflect their variable incorporation into parent bodies forming at different times and/or in different places, following injection into the early solar nebula (Yada et al. 2008). Busemann et al. (2009) did not identify any group 4 grains in their study of Grigg-Skjellerup collector IDPs, but did find four rare ^{17}O-depleted group 3 grains in the IDP L2054 G4. Nittler et al. (2008) argued that such grains are related to ^{18}O-rich group 4 grains and probably have a supernova origin as well. If this is the case, the high abundance of these grains in this IDP may also provide support for the supernova injection scenario.

C and N Isotopic Anomalies in IDPs

Carbonaceous matter with C isotopic anomalies of a likely non-nuclear origin (i.e., not produced by stellar nucleosynthesis) was first observed in IDPs (Floss et al. 2004, 2006) and has since been found in primitive meteorites as well (e.g., Busemann et al. 2006; Floss and Stadermann 2009b), although it remains relatively rare. This matter is typically also anomalous in N. Carbonaceous material characterized by N and/or H anomalies, but without C isotopic anomalies, is much more abundant and is well-known from IDPs as well as primitive meteorites (e.g., Messenger 2000; Aléon et al.

Table 4. Auger elemental compositions (atom%) of ^{15}N-rich regions in the IDP Andric.

		O	Si	Mg	Fe	Al	C	N	S	O	C	N	
Sample [a]	#[b]	Original compositions								Renormalized values[c]			N/C
1–6 hs1	1	19 ± 1	45 ± 5	b.d.	b.d.	b.d.	27 ± 30	8.5 ± 0.9	b.d.	34 ± 1	50 ± 6	16 ± 2	0.31
1–6 hs2	1	23 ± 1	41 ± 4	b.d.	2.8 ± 0.3	b.d.	25 ± 3	9.0 ± 1.0	b.d.	40 ± 1	44 ± 5	16 ± 2	0.37
2–6 hs1	1	22 ± 1	23 ± 3	4.2 ± 0.4	5.6 ± 0.6	b.d.	41 ± 4	3.3 ± 0.4	1.7 ± 0.2	33 ± 1	62 ± 7	5.0 ± 0.5	0.08
3–3 hs1	1	37 ± 1	19 ± 2	8.0 ± 0.8	3.6 ± 0.4	b.d.	26 ± 3	2.2 ± 0.2	5.1 ± 0.5	57 ± 2	40 ± 4	3.3 ± 0.4	0.08
1–1 areas	2	40–45	24–28	4.2–5.0	5.4–5.5	b.d.	15–24	1.3–2.1	b.d.–1.4	70–72	25–37	2.0–3.3	0.06–0.14
1–2 areas	3	23–35	24–39	6.4–13	b.d.–4.9	b.d.	25–35	1.3–1.5	b.d.	46–56	41–51	2.0–2.9	0.04–0.06
1–3 areas	5	12–21	32–59	b.d.–3.6	b.d.	b.d.	26–46	1.4–2.8	b.d.–1.5	23–34	63–74	2.1–6.7	0.03–0.10
1–5 areas	1	35	33	4.2	5.5	b.d.	21	2.1	b.d.	60	36	3.6	0.10
1–6 areas	7	19–36	24–49	b.d.–8.4	b.d.–7.8	b.d.	17–27	5.9–9.6	b.d.–1.2	34–59	30–50	10–19	0.31–0.52
2–1 areas	1	15	26	2.4	5.4	b.d.	50	1.6	b.d.	23	75	2.5	0.03
2–6 areas	20	9.0–28	9.6–56	b.d.–6.8	b.d.–8.8	b.d.	30–73	1.9–4.9	b.d.–4.3	14–41	53–84	2.4–11	0.03–0.16
3–3 areas	20	23–44	13–25	b.d.–8.9	b.d.–9.3	b.d.–4.6	19–54	1.8–3.3	b.d.–5.1	29–67	29–68	2.4–5.6	0.04–0.15

[a]Designation refers to the wafer and specific slice analyzed (note that the numbering does not imply adjacent slices); "hs" refers to hotspots in a given slice.
[b]Number of regions analyzed.
[c]Compositions renormalized for O, C, and N only; see text for details.
b.d. = below detection.

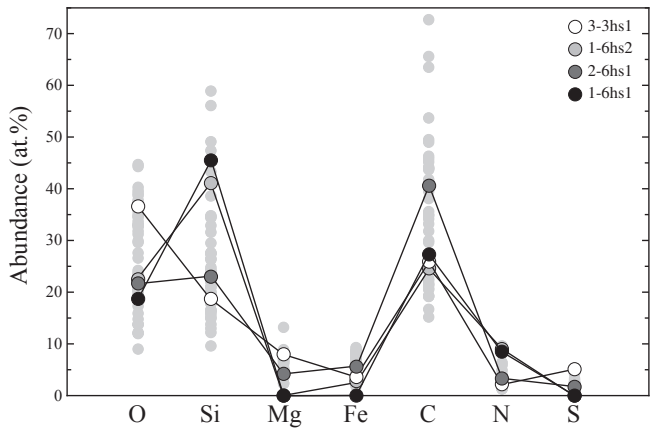

Fig. 5. Range of elemental compositions observed in isotopically anomalous (^{15}N-rich) regions of slices from the IDP Andric. Unlabeled light circles indicate data from diffuse isotopically anomalous regions in Andric; labeled circles indicate data from discrete ^{15}N-rich hotspots.

2001, 2003; Busemann et al. 2006; Floss et al. 2006; Floss and Stadermann 2009d). Recent work shows that organic nanoglobules are one major carrier of these anomalies in carbonaceous chondrites such as Tagish Lake and Bells, as well as in some IDPs (Nakamura-Messenger et al. 2006; Messenger et al. 2008). It has generally been thought that this matter formed in cold molecular clouds via low temperature ion-molecule reactions (e.g., Messenger 2000). Nitrogen self-shielding in the nebular disk has also been proposed as an alternative source for the ^{15}N enrichments seen in extraterrestrial matter (Clayton 2002a,b), although current models only predict enrichments significantly lower than those observed in IDPs and primitive meteorites (Lyons et al. 2009). Floss et al. (2006) and Floss and Stadermann (2009b) reviewed at length the formation of N and C isotopic anomalies through ion-molecule exchange reactions in cold molecular clouds (e.g., Langer et al. 1984; Langer and Graedel 1989; Terzieva and Herbst 2000; Rodgers and Charnley 2008). A key observation is that the presence of both ^{13}C-enriched and ^{13}C-depleted grains indicates that a variety of reactions contribute to the formation of interstellar carbonaceous matter (Floss and Stadermann 2009b). Similarly, although most N-anomalous hotspots are ^{15}N-rich, ^{15}N-depleted regions are occasionally also observed (Messenger 2000; Nittler et al. 2005; Floss and Stadermann 2009d; Floss et al. 2009), indicating that multiple reaction pathways are probably also involved in interstellar N chemistry.

Andric contains numerous ^{15}N-rich hotspots, three of which also exhibit C isotopic anomalies (Table 3; Fig. 4). The maximum δ^{15}N values of +940‰ in Andric are close to those observed previously in IDPs (Floss et al. 2006; Busemann et al. 2009), but fall short, by more than a factor of three, of the maximum ^{15}N enrichments of +3200‰ observed in the CM2 chondrite Bells (Busemann et al. 2006). All three of the C-anomalous hotspots are enriched in ^{13}C (Fig. 4), whereas the majority of the carbonaceous grains with C isotopic anomalies found to date are depleted in ^{13}C (Floss et al. 2004; Busemann et al. 2006; Floss and Stadermann 2009b). However, one other ^{13}C-rich hotspot has been identified in an IDP (Floss et al. 2006) and several isotopically anomalous carbonaceous grains from QUE 99177 and MET 00426 are ^{13}C-rich, including the first C-anomalous nanoglobule (Floss and Stadermann 2009b). In addition, we noted earlier that the data for Andric seem to suggest a correlation between C and N isotopic compositions. Such a trend has not previously been observed in IDPs (Floss et al. 2006) or in isotopically anomalous carbonaceous matter from primitive meteorites (Floss and Stadermann 2009b). A recent synthesis of available C and N isotopic data for various comets (Schultz et al. 2008) indicates typical enrichments in ^{15}N of approximately 1000‰ relative to the terrestrial value (average ^{14}N/^{15}N = 141 ± 29), very similar to maximum enrichments observed in ^{15}N-rich hotspots from Andric (Fig. 4). Measured cometary C isotopic ratios are consistent with the terrestrial value within errors (average ^{12}C/^{13}C = 91 ± 21), but with sufficient variation among individual comets (^{12}C/^{13}C varies between 34 and 135) to incorporate the relatively modest ^{13}C enrichments observed in Andric. Samples from comet 81P/Wild 2 also show solar C isotopic compositions, but contain isotopically heavy N, with hotspots enriched in ^{15}N up to 1300‰ (McKeegan et al. 2006; Stadermann et al. 2008). If the isotopically heavy component in Andric originates from a single, possibly cometary, source with a uniform composition, then the trend observed in Fig. 4 could result from mixing between this component and one with normal (terrestrial) C and N isotopic compositions. However, elemental data obtained by Auger spectrometry suggest that while isotopic dilution does appear to play a role, a variety of components may be hosting the isotopic anomalies observed (see below).

Floss et al. (2006) observed that IDPs with anomalous bulk N isotopic compositions tend to have lower bulk CN^-/C^- ratios than IDPs with isotopically normal N, and the most N-anomalous IDPs have the lowest CN^-/C^- ratios. However, it is difficult to directly infer the actual N/C abundance ratio from these secondary ion yields: because N is measured as CN^- in SIMS, the formation of this cluster depends not only on the presence of both C and N, but probably also on the exact nature of the analyzed material (e.g., matrix

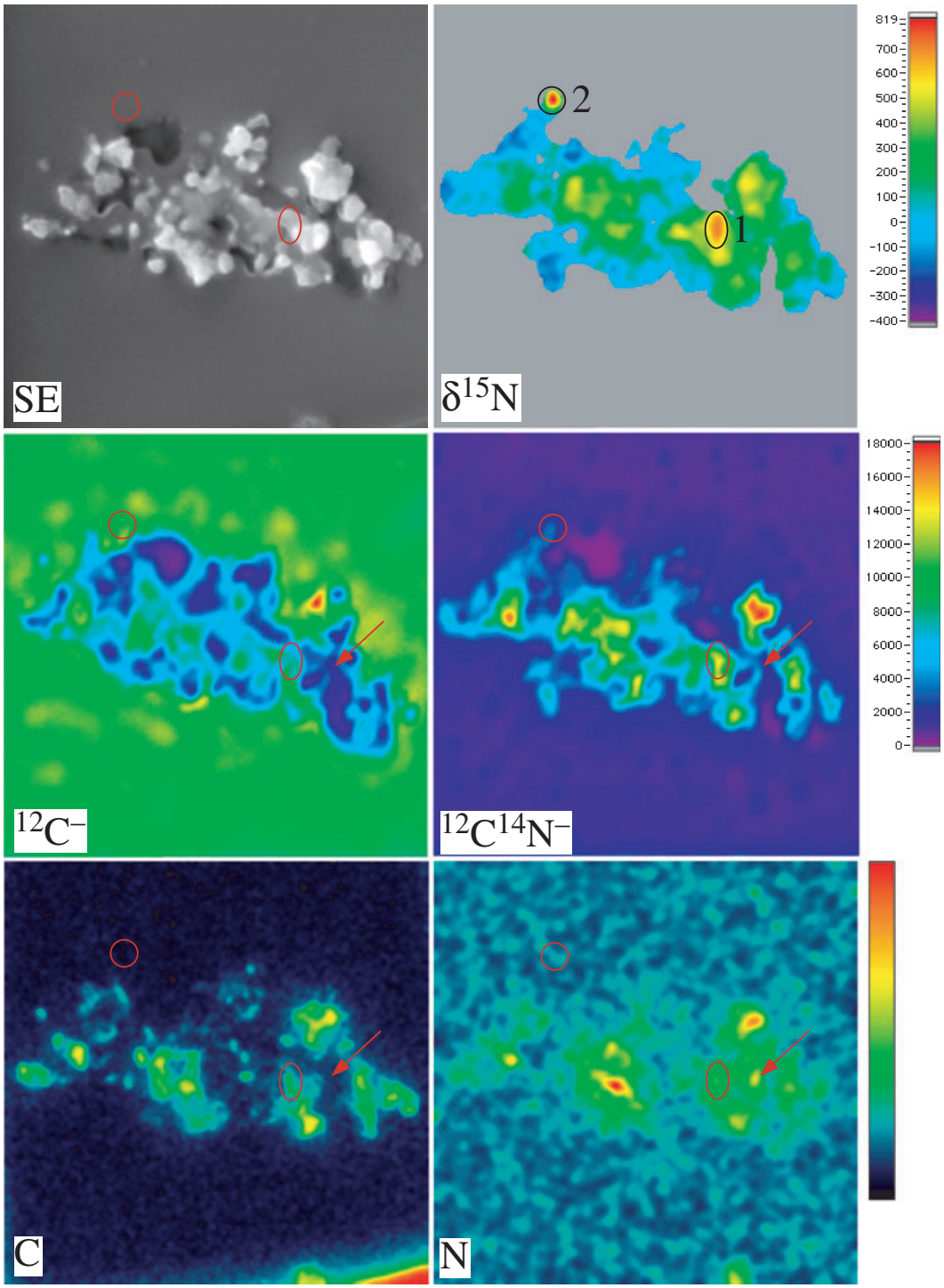

Fig. 6. Slice 3–3 of the IDP Andric showing the locations of two ^{15}N-rich hotspots. Top: field emission secondary electron image and false-color map of δ^{15}N. Middle: false-color NanoSIMS $^{12}C^-$ and $^{12}C^{14}N^-$ ion images. Bottom: false-color Auger C and N elemental maps. Note that hotspot 2 sputtered away during the NanoSIMS measurement. See text for discussion of the region indicated by the arrow. Field of view is approximately 5 μm across.

effects). By using Auger spectrometry to map C and N elemental distributions and to measure their concentrations in discrete subgrains, we are able to circumvent this issue of N quantification in SIMS. The elemental distributions shown in Fig. 6 for slice 3–3 show that hotspot 1, with a ^{13}C enrichment and one of

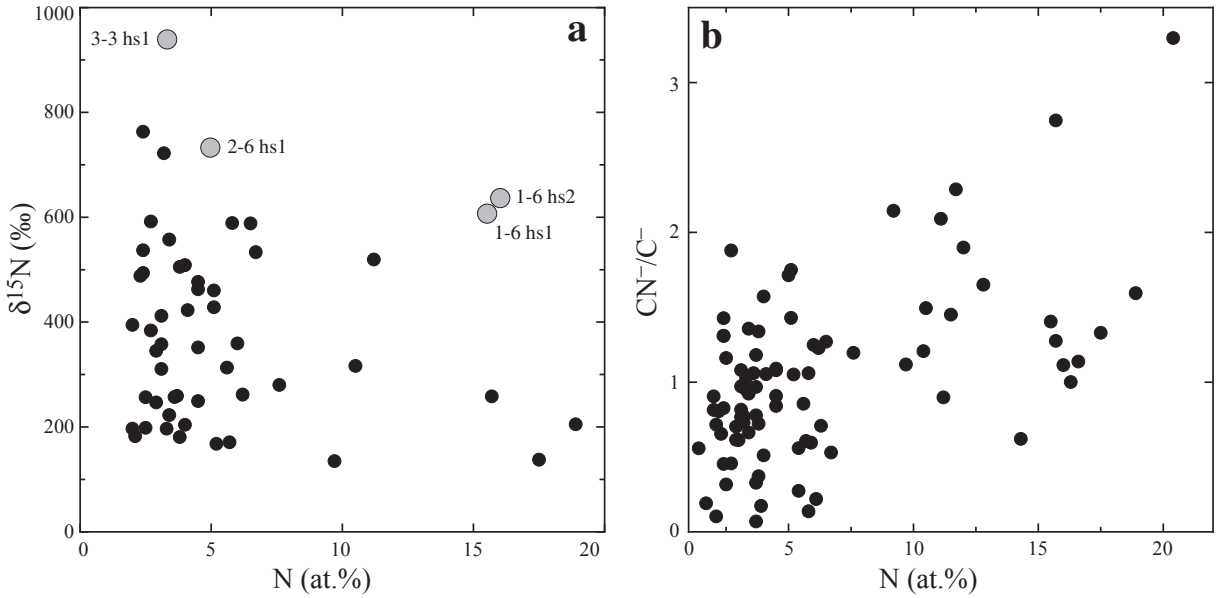

Fig. 7. Normalized Auger N abundances (atom%) versus N isotopic compositions (a) and NanoSIMS CN^-/C^- ratios (b) in the IDP Andric. Panel (b) shows data from all regions analyzed in the IDP, whereas panel (a) only shows data for areas with isotopically anomalous N compositions. Hotspots are shown as light gray circles.

the highest ^{15}N enrichments in Andric (Table 3), contains both C and N. The Auger elemental spectrum confirms the presence of these elements (Table 4), but also shows that O and Si are present, as well as minor amounts of Fe, Mg, and S. As discussed above, this likely reflects an intimate intermingling of carbonaceous matter, hosting the C and N isotopic anomalies observed in this hotspot, along with silicates and sulfides. Similar fine-scale intermingling of solar and presolar components in IDPs has been noted in other studies (e.g., Keller et al. 2004). As noted earlier, Fig. 6 also shows that although C and N are both present in most parts of this slice, there are some exceptions, such as the region indicated by the arrow, which is N-rich, but contains little C. Moreover, although hotspot 1 contains both C and N, abundances of these elements are higher in other parts of the IDP with less anomalous N isotopic compositions.

The acquisition of Auger elemental spectra and the determination of sensitivity factors for C and N through analysis of kerogen materials (see the Experimental section) allows us to quantify the C and N abundances and compare them directly with the N isotopic compositions in Andric. Carbon abundances vary widely in the hotspots and diffuse anomalous areas, from about 25 to 85 atom% (Table 4), while nitrogen concentrations in these areas range up to 19 atom%. N/C ratios range from values similar to those seen in the CR and CM chondrites (at. N/C approximately 0.03; Alexander et al. 2007) to values that are an order of magnitude higher (Table 4). However, there is no obvious correlation between C and N abundances in the areas. One explanation for these variations is that a variety of carbonaceous components carry the N (and occasional C) isotopic anomalies observed. A similar conclusion was reached by Busemann et al. (2009) for several primitive IDPs they studied from one of the Grigg-Skjellerup collectors. In addition, Cody et al. (2008) noted that the wide chemical range observed for organic matter from comet 81P/Wild 2 was likely to indicate multiple origins. However, another possibility for Andric is that its carbonaceous matter originates from a single (possibly cometary) source, as suggested above, and that dilution is responsible for the range of compositions observed. Unlike Busemann et al. (2009), who did not see a correlation between isotopic and elemental compositions, we do observe a relationship between N isotopic compositions and elemental abundance. Figure 7a shows a wide range of N isotopic compositions at low N abundances and a decrease in the range of $\delta^{15}N$ enrichments with increasing N abundances. For example, the most anomalous hotspots, 3–3 hs1 and 2–6 hs1, exhibit relatively low N abundances (on the order of 5 atom% or less), whereas hotspots 1–6 hs1 and 1–6 hs2, which are less enriched in ^{15}N, have significantly higher N abundances. Shown in Fig. 7b are N abundances determined from Auger spectroscopy plotted against CN^-/C^- ratios from the NanoSIMS measurements. Although there is considerable scatter, in general N abundances are positively correlated with CN^-/C^-. In addition, Fig. 8 shows that there is a good correlation for our kerogen

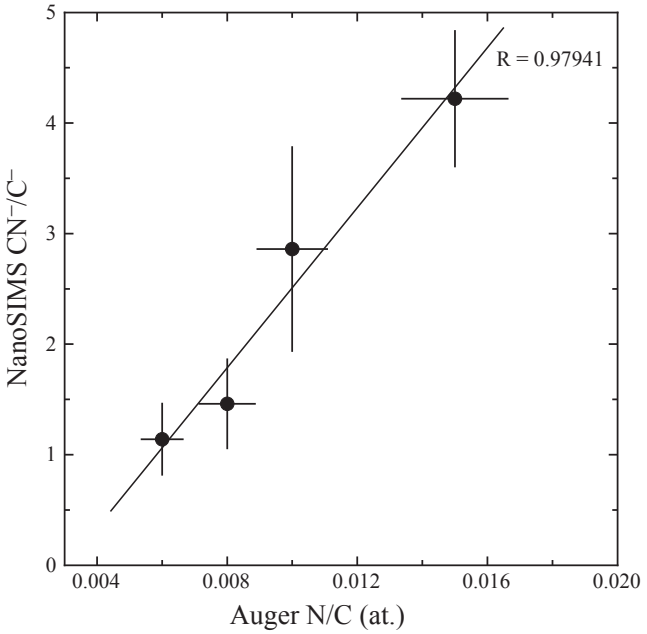

Fig. 8. Auger N/C ratios versus NanoSIMS CN^-/C^- ratios for terrestrial kerogen standards.

standards between the N/C ratios obtained from the Auger measurements and the CN^-/C^- ratios measured in the NanoSIMS, indicating that these ion ratios provide a fairly robust indication of relative N contents, at least in single phase materials. The greater degree of scatter observed in the IDP data is likely due to the fact that the areas analyzed do not consist of single phases, but rather are a mix of different materials with differing ionization efficiencies for the CN molecule. Because Auger spectroscopy is a surface-sensitive technique, it is important to note that the trends exhibited in Figs. 7b and 8 demonstrate that the N abundances determined by Auger spectroscopy are intrinsic to the phases analyzed and are not dominated by surface contamination.

The range of N isotopic compositions at low N abundances suggests that the isotopic anomalies are indeed hosted a variety of carbonaceous components that are relatively N-poor. As N concentrations increase, the range in the magnitude of the anomalies decreases, suggesting that contamination with isotopically normal N may be diluting the isotopic anomalies. This dilution could arise from a variety of sources, including extraterrestrial as well as terrestrial ones. Although the correlation between NanoSIMS CN^-/C^- ratios and Auger N abundances indicates that surface contamination during the Auger measurements is not responsible, we cannot completely rule out other forms of laboratory contamination. The epoxy in which these IDPs were embedded for slicing is one possible source of this contamination; however, our NanoSIMS data indicate that the CN^-/C^- ratios of the resin (0.06–0.23) surrounding the IDPs are well below the ratios observed for the IDPs themselves (Table 3), indicating that N abundances and isotopic compositions are not significantly affected by the surrounding resin. In addition, the fact that a similar relationship was observed by Floss et al. (2006) for bulk IDPs that were prepared differently (pressed as whole particles into high purity Au rather than sliced in epoxy and mounted on Si wafers) suggests that this dilution is more likely to have originated either extraterrestrially or during atmospheric entry of the particles.

Isotopically Primitive IDPs

Andric is a member of the isotopically primitive subgroup of IDPs (Floss et al. 2006), with all the defining characteristics of other particles from this group: isotopically anomalous bulk N compositions; abundant ^{15}N-rich hotspots, some of which also exhibit C isotopic anomalies; and a high abundance of O-anomalous presolar grains. In contrast, IDPs Perse and Quasimodo both have normal N isotopic compositions and lack presolar grains, similar to other IDPs studied by Floss et al. (2006). As noted earlier, Perse and Quasimodo both come from collectors flown in April 2003 through the Grigg-Skjellerup comet debris trail. Busemann et al. (2009) recently argued for a Grigg-Skjellerup origin for two primitive IDPs they studied from the G-S collector L2054. Both IDPs contain high abundances of presolar grains, have anomalous H and N isotopic compositions with abundant D and ^{15}N-enrichments, and contain primitive organic matter whose Raman signatures indicate little thermal alteration. However, other G-S collector IDPs studied by these authors appear, like Perse and Quasimodo from this work, to be less primitive. Andric comes from collector U2108, which flew during the Leonid showers in November 2002 in an effort to collect particles from comet 55P/Tempel-Tuttle. Rietmeijer et al. (2003) noted that particles from this comet are expected to be molten due to their high entry velocity (approximately 72 km s^{-1} versus approximately 12–20 km s^{-1} for typical IDPs; Brownlee et al. 1995). However, the high concentrations of presolar grains in Andric, coupled with the presence of isotopically anomalous carbonaceous matter, including some material with C isotopic anomalies, indicates that this IDP clearly did not experience high temperatures during atmospheric entry.

Interplanetary dust particles from many different sources will be collected even on "dedicated collectors" that are designed to capture particles from a targeted

cometary dust trail, and the provenance of any given IDP is necessarily uncertain. For example, Messenger (2002) noted that the flux of particles expected from Grigg-Skjellerup in the time frame during which the collectors were flown was likely to be on the order of a few percent of the background IDP flux. Thus, while highly primitive IDPs found on these collectors may indeed come from the comet Grigg-Skjellerup, as suggested by Busemann et al. (2009), it is not surprising that other IDPs sampled from these collectors represent a variety of types, with some particles exhibiting less primitive characteristics than others. In addition, primitive IDPs, with high presolar grain abundances and isotopically anomalous H and N compositions are also common on nontargeted collectors (e.g., Messenger et al. 2003a, 2003b; Floss et al. 2006), suggesting that a variety of sources have preserved this type of primitive material. Indeed, similarly primitive material is also found in the most unaltered meteorites, such as the CR3 chondrites QUE 99177 and MET 00426, which contain high abundances of presolar grains and carbonaceous matter with C and N isotopic anomalies similar to those observed in isotopically primitive IDPs (Floss and Stadermann 2009a, 2009b, 2009d). Raman work on the insoluble organic matter (IOM) in these primitive meteorites and IDPs shows that the isotopic anomalies are carried by the most pristine and thermally unaltered IOM (Busemann et al. 2006, 2007; Alexander et al. 2007).

The presence of pristine IOM, with abundant H, N, and C isotopic anomalies, and high abundances of presolar grains in primitive IDPs is consistent with their postulated origin from comets, which accreted at low temperatures in the outer solar system. However, meteorites such as the CR chondrites, which contain similarly pristine and isotopically anomalous IOM, are thought to have originated in the asteroid belt. Reports have suggested the presence of icy, comet-like planetesimals in the outer asteroid belt (e.g., Hsieh and Jewitt 2006) and recent observations have confirmed the presence of water ice and organic material on the surface of one such "Main Belt comet," asteroid 24 Themis (Campins et al. 2010; Rivkin and Emery 2010). Based on dynamical considerations, Hsieh and Jewitt (2006) argued for accretion of these bodies in this region of the solar nebula, implying that the snow line was once within the asteroid belt. More recently, Levison et al. (2009) modeled the dynamical evolution of objects that originally formed in the primordial cometary disk and found that a significant fraction of trans-Neptunian objects are captured in the outer asteroid belt, providing an alternate source for these Main Belt comets. Both scenarios would provide a mechanism by which the IOM in primitive meteorites, such as the CR chondrites, could have been shielded from higher temperatures prior to incorporation into the meteorite parent bodies. In addition, the existence of Main Belt comets opens the possibility that the primitive IDPs sampled in the Earth's stratosphere may not necessarily come directly from the outer solar system. Levison et al. (2009) noted that these volatile-rich captured bodies would be more susceptible to collisional evolution than typical Main Belt asteroids, and could be an important source of dust captured by the Earth. Stepped He release can be used to determine atmospheric entry velocities of IDPs and, thus, distinguish between cometary (high velocity, strongly heated) and asteroidal (low velocity, weakly heated) particles; Brownlee et al. (1995) used this approach and noted that their population of cometary particles was dominated by chondritic porous IDPs. However, the cometary origin of most IDPs has been inferred from isotopic, mineralogical, and/or textural characteristics, leaving open the possibility that they may, in fact, come from the outer asteroid belt. The fact that the total population of IDPs shows such a wide, but seemingly continuous, variation from very primitive particles rich in presolar grains to more altered, presolar-grain-free particles may, thus, simply be a reflection of the continuous transition in possible parent bodies from primitive asteroids to Main Belt comets to typical Kuiper Belt comets.

Acknowledgments—We thank Tim Smolar for maintenance of the Washington University NanoSIMS and Auger Nanoprobe. We are grateful to L. Nittler and S. Messenger for careful reviews which substantially improved this paper. This work was supported by NASA grants NNG07AI45G and NNX10AI64G (C. Floss, PI), and NNX08AI13G (F. J. Stadermann, PI).

Editorial Handling—Dr. Ian Franchi

REFERENCES

Aléon J., Engrand C., Robert F., and Chaussidon M. 2001. Clues to the origin of interplanetary dust particles from the isotopic study of their hydrogen-bearing phases. *Geochimica et Cosmochimica Acta* 65:4399–4412.

Aléon J., Robert F., Chaussidon M., and Marty B. 2003. Nitrogen isotopic composition of macromolecular organic matter in interplanetary dust particles. *Geochimica et Cosmochimica Acta* 67:3773–3787.

Alexander C. M. O'D., Fogel M., Yabuta H., and Cody G. D. 2007. The origin and evolution of chondrites recorded in the elemental and isotopic compositions of their macromolecular organic matter. *Geochimica et Cosmochimica Acta* 71:4380–4403.

Bradley J. P. 1994. Chemically anomalous preaccretionally irradiated grains in interplanetary dust from comets. *Science* 265:925–929.

Brownlee D. E., Joswiak D. J., Schlutter D. J., Pepin R. O., Bradley J. P., and Love S. G. 1995. Identification of individual cometary IDPs by thermally stepped He release. Proceedings, 26th Lunar and Planetary Science Conference. pp. 183–184.

Brownlee D., Tsou P., Aléon J., Alexander C. M. O'D., Araki T., Bajt S., Baratta G. A., Bastien R., Bland P., Bleuet P., Borg J., Bradley J. P., Brearley A., Brenker F., Brennan S., Bridges J. C., Browning N., Brucato J. R., Brucato H., Bullock E., Burchell M. J., Busemann H., Butterworth A., Chaussidon M., Cheuvront A., Chi M., Cintal M. J., Clark B. C., Clemett S. J., Gody G., Colangeli L., Cooper G., Cordier P., Daghlian C., Dai Z. R., d'Hendecourt L., Djouadi Z., Dominguez G., Duxbury T., Dworkin J. P., Ebel D., Economou Th. E., Fakra S., Fairey S. A. J., Fallon S., Ferrini G., Ferroir T., Fleckenstein H., Floss C., Flynn G., Franchi I. A., Fries M., Gainsforth Z., Gallien J.-P., Genge M., Gilles M. K., Gillet Ph., Gilmour J., Glavin D. P., Gounelle M., Grady M. M., Graham G. A., Grant P. G., Green S. F., Grossemy F., Grossman L., Grossman J. N., Guan Y., Hagiya K., Harvey R., Heck Ph., Herzog G. F., Hoppe P., Hörz F., Huth J., Hutcheon I. D., Ignatyev K., Ishii H., Ito M., Jacob D., Jacobsen C., Jacobsen S., Jones S., Joswiak D., Jurewicz A., Kearsley A. T., Keller L. P., Khodja H., Kilcoyne A. L. D., Kissel J., Krot A., Langenhorst F., Lanzirotti A., Le L., Leshin L. A., Leitner J., Lemelle L., Leroux H., Liu M.-C., Luening K., Lyon I., MacPherson G., Marcus M. A., Marhas K., Marty B., Matrajt G., McKeegan K., Meibom A., Mennella V., Messenger K., Messenger S., Mikouchi T., Mostefaoui S., Nakamura T., Nakano T., Newville M., Nittler L. R., Ohnishi I., Ohsumi K., Okudaira K., Papanastassiou D. A., Palma R., Palumbo M. E., Pepin R. O., Perkins D., Perronnet M., Pianetta P., Rao W., Rietmeijer F. J. M., Robert F., Rost D., Rotundi A., Ryan R., Sandford S. A., Schwandt C. S., See T. H., Schlutter D., Sheffield-Parker J., Simionovici A., Simon S., Sitnitsky I., Snead C. J., Spencer M. K., Stadermann F. J., Steele A., Stephan T., Stroud R., Susini J., Sutton S. R., Suzuki Y., Taheri M., Taylor S., Teslich N., Tomeoka K., Tomioka N., Toppani A., Trigo-Rodríguez J. M., Troadec D., Tsuchiyama A., Tuzzolino A. J., Tyliszczak T., Uesugi K., Velbel M., Vellenga J., Vicenzi E., Vincze L., Warren J., Weber I., Weisberg M., Westphal A. J., Wirick S., Wooden D., Wopenka B., Wozniakiewicz P., Wright I., Yabuta H., Yano H., Young E. D., Zare R. N., Zega T., Ziegler K., Zimmerman L., Zinner E., and Zolensky M. 2006. Comet 81P/Wild 2 under a microscope. *Science* 314:1711–1716.

Busemann H., Young A. F., Alexander C. M. O'D., Hoppe P., Mukhopadhyay S., and Nittler L. R. 2006. Interstellar chemistry recorded in organic matter from primitive meteorites. *Science* 312:727–730.

Busemann H., Alexander C. M. O'D., and Nittler L. R. 2007. Characterization of insoluble organic matter in primitive meteorites by microRaman spectroscopy. *Meteoritics & Planetary Science* 42:1387–1416.

Busemann H., Nguyen A. N., Cody G. D., Hoppe P., Kilcoyne A. L. D., Stroud R. M., Zega T. J., and Nittler L. R. 2009. Ultra-primitive interplanetary dust particles from the comet 26P/Grigg-Skjellerup dust stream collection. *Earth and Planetary Science Letters* 288:44–57.

Campins H., Hargrove K., Pinilla-Alonso N., Howell E. S., Kelley M. S., Licandro J., Mothé-Diniz T., Fernández Y., and Ziffer J. 2010. Water ice and organices on the surface of the asteroid 24 Themis. *Nature* 464:1320–1321.

Ciesla F. J. 2009. Two-dimensional transport of solids in viscous protoplanetary disks. *Icarus* 200:655–671.

Clayton R. N. 2002a. Self-shielding in the solar nebula. *Nature* 415:860–861.

Clayton R. N. 2002b. Nitrogen isotopic fractionation by photochemical self-shielding. *Meteoritics & Planetary Science* 37:A35.

Cody G. D., Ade H., Alexander C. M. O'D., Araki T., Butterworth A., Fleckenstein H., Flynn G., Gilles M. K., Jacobsen C., Kilcoyne A. L. D., Messenger K., Sandford S. A., Tyliczszak T., Westphal A. J., Wirick S., and Yabuta H. 2008. Quantitative organic and light-element analysis of comet 81P/Wild 2 particles using C-, N-, and O-μ-XANES. *Meteoritics & Planetary Science* 43:353–365.

Croat T. K., Bernatowicz T., Amari S., Messenger S., and Stadermann F. J. 2003. Structural, chemical, and isotopic microanalytical investigations of graphite from supernovae. *Geochimica et Cosmochimica Acta* 67:4705–4725.

Floss C. and Stadermann F. J. 2009a. Auger Nanoprobe analysis of presolar ferromagnesian silicate grains from primitive CR chondrites QUE 99177 and MET 00426. *Geochimica et Cosmochimica Acta* 73:2415–2440.

Floss C. and Stadermann F. J. 2009b. High abundances of circumstellar and interstellar C-anomalous phases in the primitive CR3 chondrites QUE 99177 and MET 00426. *The Astrophysical Journal* 697:1242–1255.

Floss C. and Stadermann F. J. 2009c. The presolar grain inventories of Adelaide and Kakangari. *Geochimica et Cosmochimica Acta* 73:A385.

Floss C. and Stadermann F. J. 2009d. Interstellar components in the primitive CR3 chondrites QUE 99177 and MET 00426 (abstract #1083). 40th Lunar and Planetary Science Conference. CD-ROM.

Floss C., Stadermann F. J., Bradley J. P., Dai Z. R., Bajt S., and Graham G. 2004. Carbon and nitrogen isotopic anomalies in an anhydrous interplanetary dust particle. *Science* 303:1355–1358.

Floss C., Stadermann F. J., Bradley J. P., Dai Z. R., Bajt S., Graham G., and Lea A. S. 2006. Identification of isotopically primitive interplanetary dust particles: A NanoSIMS isotopic imaging study. *Geochimica et Cosmochimica Acta* 70:2371–2399.

Floss C., Stadermann F. J., Mertz A., and Bernatowicz T. 2007. Anatomy of an isotopically primitive interplanetary dust particle: Coordinated NanoSIMS and Auger Nanoprobe analyses (abstract #1145). 38th Lunar and Planetary Science Conference. CD-ROM.

Floss C., Stadermann F. J., Yada T., Noguchi T., and Nakamura T. 2009. Anomalous nitrogen isotopic compositions in the stardust-rich Antarctic micrometeorite T98G8: Affinities to primitive CR chondrites and anhydrous IDPs (abstract #1082). 40th Lunar and Planetary Science Conference. CD-ROM.

Floss C., Stadermann F. J., Mertz A. F., and Wopenka B. 2010. Anatomy of an isotopically primitive IDP from the 55P/Tempel-Tuttle targeted collector: Quantitative Auger measurements of C and N abundances in N-anomalous hotspots (abstract #1330). 41st Lunar and Planetary Science Conference. CD-ROM.

Hayes J. M., Kaplan I. R., and Wedeking K. W. 1983. Precambrian organic geochemistry, preservation of the record. In *Earth's earliest biosphere: Its origin and evolution*, edited by Schopf J. W. Princeton, NJ: Princeton University. pp. 93–134.

Hsieh H. H. and Jewitt D. 2006. A population of comets in the main asteroid belt. *Science* 312:561–563.

Keller L. P., Messenger S., Flynn G. J., Clemett S. J., Wirick S., and Jacobsen C. 2004. The nature of molecular cloud material in interplanetary dust. *Geochimica et Cosmochimica Acta* 68:2577–2589.

Langer W. D. and Graedel T. E. 1989. Ion-molecule chemistry of dense interstellar clouds: Nitrogen-, oxygen-, and carbon-bearing molecule abundances and isotopic ratios. *The Astrophysical Journal Supplement Series* 69:241–269.

Langer W. D., Graedel T. E., Frerking M. A., and Armentrout P. B. 1984. Carbon and oxygen isotope fractionation in dense molecular clouds. *The Astrophysical Journal* 277:581–604.

Levison H. F., Bottke W. F., Gounelle M., Morbidelli A., Nesvorny D., and Tsiganis K. 2009. Contamination of the asteroid belt by primordial trans-Neptunian objects. *Nature* 460:364–366.

Lyons J. R., Bergin E. A., Ciesla F. J., Davis A. M., Desch S. J., Hashizume K., and Lee J.-E. 2009. Timescales for the evolution of oxygen isotope compositions in the solar nebula. *Geochimica et Cosmochimica Acta* 73:4998–5017.

McKeegan K. D., Aléon J., Bradley J., Brownlee D., Busemann H., Butterworth A., Chaussidon M., Fallon S., Floss C., Gilmour J., Gounelle M., Graham G., Guan Y., Heck P. R., Hoppe P., Hutcheon I. D., Huth J., Ishii H., Ito M., Jacobsen S. B., Kearsley A., Leshin L. A., Liu M.-C., Lyon I., Marhas K., Marty B., Matrajt G., Meibom A., Messenger S., Mostefaoui S., Mukhopadhyay S., Nakamura-Messenger K., Nittler L., Palma R., Pepin R. O., Papanastassiou D. A., Robert F., Schlutter D., Snead C. J., Stadermann F. J., Stroud R., Tsou P., Westphal A., Young E. D., Ziegler K., Zimmermann L., and Zinner E. 2006. Isotopic compositions of cometary matter returned by Stardust. *Science* 314:1724–1728.

Messenger S. 2000. Identification of molecular-cloud material in interplanetary dust particles. *Nature* 404:968–971.

Messenger S. 2002. Opportunities for the stratospheric collection of dust from short-period comets. *Meteoritics & Planetary Science* 37:1491–1505.

Messenger S., Stadermann F. J., Floss C., Nittler L. R., and Mukhopadhyay S. 2003a. Isotopic signatures of presolar materials in interplanetary dust. *Space Science Reviews* 106:155–172.

Messenger S., Keller L. P., Stadermann F. J., Walker R. M., and Zinner E. 2003b. Samples of stars beyond the solar system: Silicate grains in interplanetary dust. *Science* 300:105–108.

Messenger S., Keller L. P., and Lauretta D. S. 2005. Supernova olivine from cometary dust. *Science* 309:737–741.

Messenger S., Nakamura-Messenger K., and Keller L. P. 2008. ^{15}N-rich organic globules in a cluster IDP and the Bells CM2 chondrite (abstract #2391). 39th Lunar and Planetary Science Conference. CD-ROM.

Nakamura-Messenger K., Messenger S., Keller L. P., Clemett S. J., and Zolensky M. E. 2006. Organic globules in the Tagish Lake meteorite: Remnants of the protosolar disk. *Science* 314:1439–1442.

Nguyen A. N., Stadermann F. J., Zinner E., Stroud R. M., Alexander C. M. O'D., and Nittler L. R. 2007. Characterization of presolar silicate and oxide grains in primitive carbonaceous chondrites. *The Astrophysical Journal* 656:1223–1240.

Nittler L. R. 2007. Presolar grain evidence for low-mass supernova injection into the solar nebula. Workshop on the Chronology of Meteorites and the Early Solar System. pp. 125–126.

Nittler L. R., Alexander C. M. O'D., Gao X., Walker R. M., and Zinner E. 1997. Stellar sapphires: The properties and origins of presolar Al_2O_3 in meteorites. *The Astrophysical Journal* 483:475–495.

Nittler L. R., Hoppe P., Alexander C. M. O'D., Busemann H., and Cody G. 2005. Extensive microscale N isotopic heterogeneity in chondritic organic matter (abstract). *Meteoritics & Planetary Science* 40:A114.

Nittler L. R., Alexander C. M. O'D., Gallino R., Hoppe P., Nguyen A. N., Stadermann F. J., and Zinner E. K. 2008. Aluminum-, calcium- and titanium-rich oxide stardust in ordinary chondrite meteorites. *The Astrophysical Journal* 682:1450–1478.

Palma R. L., Pepin R., and Schlutter D. J. 2005. Helium and neon isotopic compositions from IDPs of potentially cometary origin (abstract). *Meteoritics & Planetary Science* 40:A120.

Rietmeijer F. J. M., Pfeffer M. A., Chizmadia L. J., Macy B., Fischer T. P., Zolensky M. E., Warren J. L., and Jenniskens P. 2003. Leonid dust spheres captured during the 2002 storm? (abstract #1358). 34th Lunar and Planetary Science Conference. CD-ROM.

Rivkin A. S. and Emery J. P. 2010. Detection of ice and organics on an asteroidal surface. *Nature* 464:1322–1323.

Rodgers S. D. and Charnley S. B. 2008. Nitrogen superfractionation in dense cloud cores. *Monthly Notices of the Royal Astronomical Society* 385:L48–L52.

Schultz R., Jehin E., Manfroid J., Hutsemekers D., Arpigny C., Cochran A., Zucconi J.-M., and Stüwe J. A. 2008. Isotopic abundance in the CN coma of comets: Ten years of measurements. *Planetary and Space Science* 56:1713–1718.

Stadermann F. J., Floss C., and Wopenka B. 2006. Circumstellar aluminum oxide and silicon carbide in interplanetary dust particles. *Geochimica et Cosmochimica Acta* 70:6168–6179.

Stadermann F. J., Hoppe P., Floss C., Heck P. R., Hörz F., Huth J., Kearsley A. T., Leitner J., Marhas K. K., McKeegan K. D., and Stephan T. 2008. Stardust in Stardust—The C, N, and O isotopic compositions of Wild 2 cometary matter in Al foil impacts. *Meteoritics & Planetary Science* 43:299–313.

Stadermann F. J., Floss C., Bose M., and Lea A. S. 2009. The use of Auger spectroscopy for the in situ elemental characterization of sub-micrometer presolar grains. *Meteoritics & Planetary Science* 44:1033–1049.

Terzieva R. and Herbst E. 2000. The possibility of nitrogen isotopic fractionation in interstellar clouds. *Monthly Notices of the Royal Astronomical Society* 317:563–568.

Vollmer C., Hoppe P., Stadermann F. J., Floss C., and Brenker F. E. 2009. NanoSIMS analysis and Auger electron microscopy of silicate and oxide stardust from the carbonaceous chondrite Acfer 094. *Geochimica et Cosmochimica Acta* 73:7127–7149.

Yada T., Floss C., Stadermann F. J., Zinner E., Nakamura T., Noguchi T., and Lea A. S. 2008. Stardust in Antarctic

micrometeorites. *Meteoritics & Planetary Science* 43:1287–1298.

Zolensky M. E., Zega T. J., Yano H., Wirick S., Westphal A. J., Weisberg M. K., Weber I., Warren J. L., Velbel M. A., Tsuchiyama A., Tsou P., Toppani A., Tomioka N., Tomeoka K., Teslich N., Taheri M., Susini J., Stroud R., Stephan T., Stadermann F. J., Snead C. J., Simon S. B., Simionovici A., See T. H., Robert F., Rietmeijer F. J. M., Rao W., Perronnet M. C., Papanastassiou D. A., Okudaira K., Ohsumi K., Oshnishi I., Nakamura-Messenger K., Nakamura T., Mostefaoui S., Mikouchi T., Meibom A., Matrajt G., Marcus M. A., Leroux H., Lemelle L., Le L., Lanzirotti A., Langenhorst F., Krot A. N., Keller L. P., Kearsley A. T., Joswiak D., Jacob D., Ishii H., Harvey R., Hagiya K., Grossman L., Grossman J. N., Graham G. A., Gounelle M., Gillet P., Genge M. J., Flynn G., Ferroir T., Fallon S., Ebel D. S., Dai Z. R., Cordier P., Clark B., Chi M., Butterworth A. L., Brownlee D. E., Bridges J. C., Brennan S., Brearley A., Bradley J. P., Bleuet P., Bland P. A., and Bastien R. 2006. Mineralogy and petrology of comet 81P/Wild 2 nucleus samples. *Science* 314:1735–1739.